FULL PAPER

Solar Cells

ADVANCED
FUNCTIONAL
MATERIALS

www.afm-journal.de

PEDOT:PSS-Assisted Exfoliation and Functionalization of 2D Nanosheets for High-Performance Organic Solar Cells

Wang Xing, Yusheng Chen, Xiaoxi Wu, Xiaozhou Xu, Pan Ye, Ting Zhu, Qingyu Guo, Liqiu Yang, Weiwei Li, and Hui Huang*

Here, a facial and scalable method for efficient exfoliation of bulk transition metal dichalcogenides (TMD) and graphite in aqueous solution with poly(3,4-ethylenedioxythiophene):poly(styrenesulfonate) (PEDOT:PSS) to prepare single- and few-layer nanosheets is demonstrated. Importantly, these TMD nanosheets retain the single crystalline characteristic, which is essential for application in organic solar cells (OSCs). The hybrid PEDOT:PSS/ WS_2 ink prepared by a simple centrifugation is directly integrated as a hole extraction layer for high-performance OSCs. Compared with PEDOT:PSS, the PEDOT:PSS/WS_2-based devices provide a remarkable power conversion efficiency due to the "island" morphology and benzoid–quinoid transition. This study not only demonstrates a novel method for preparing single- and few-layer TMD and graphene nanosheets but also paves a way for their applications without further complicated processing.

1. Introduction

Graphene, an intriguing 2D nanomaterial, has attracted significant attention due to its fascinating mechanical, electronic, optical, and thermal properties since its isolation in 2004.[1] Recently, graphene analogue, transition metal dichalcogenides (TMD nanosheets) with 2D structures such as MoS_2 and WS_2 possessing obvious semiconductor bandgaps, show potential applications in electronics field.[2] The single-layer TMD nanosheets have several advantages over its bulk crystal. First, the indirect bandgap of bulk MoS_2 changes to direct in few-layer flakes.[3] Besides, the lone-pair electrons of the chalcogen atoms in the separated single-layer structure enable ballistic transport, indicating that the carrier mobility may be improved.[4] Thus, it is desirable to prepare single- and few-layer graphene/TMD nanosheets.

To date, the methods to prepare single- and few-layer graphene/TMD nanosheets mainly can be categorized into two types. One is the bottom-up method, including thermal decomposition of the precursor[5] and chemical vapor deposition,[6] which usually involves high temperatures, costly apparatus, and substrates. The other is top-down exfoliation from their bulk crystals by micromechanical cleavage,[7] chemical and electrochemical alkali metal intercalation,[8–11] and liquid exfoliation.[12–14] Micromechanical cleavage produces limited quantity of graphene/ TMD nanosheets,[7] mostly for fundamental research. Alkali metal intercalation is an efficient way to produce large-scale graphene/TMD nanosheets.[8–11] However, air-sensitive alkali metals are usually used. Moreover, the procedure requires a long reaction time, resulting in formation of unexpected by-products such as Li_2S.[15] Liquid-phase ultrasonication of bulk graphite and TMD in the presence of either organic solvent[12,13] or surfactants-containing aqueous solution[16–22] displays broad prospects to obtain single- and few-layer nanosheets. The surfactants adopted in liquid ultrasonication, including small-[16–18] or polymeric-[19–22] molecules draw increasing attention because of its environmental friendliness and safety. Once exfoliated from their bulk, graphene/TMD nanosheets can be stabilized due to the noncovalent interaction between graphene/TMD nanosheets and polymer chains, and the steric repulsion between polymer chains. For applications on electronic devices, it is necessary to remove the stabilizing polymer, which disrupts the electrical properties of graphene/TMD nanosheets.[2,23] So, it is very challenging to find a polymer that can act as a stabilizing agent and be directly applied for electronic devices.

The well-known poly(3,4-ethylenedioxythiophene):poly(styrenesulfonate) (PEDOT:PSS), widely used as hole extraction layer (HEL) for OSCs, has several disadvantages such as its hygroscopicity and acidity, which induces poor stability.[24,25] Recently, TMD nanosheets were used as HEL alternatives to PEDOT:PSS.[5,6,17,26–33] The power conversion efficiency (PCE) of OSCs based on TMD nanosheets in its original form usually can not surpass those based on the conventional interfacial extraction materials, possibly because of unexpected 2H to 1T phase transition[29] and the mismatching work function of TMD nanosheets.[17,31] To solve these problems, the TMD nanosheets films have undergone post-treatments, i.e., oxidation by hydrogen peroxide[30] to form MoO_3 nanoparticles on TMD nanosheets, UV–ozone treatment[6,27–30,33] or

W. Xing, Y. Chen, X. Wu, X. Xu, P. Ye, T. Zhu, Q. Guo,
L. Yang, Prof. H. Huang
College of Materials Science and Opto-electronic Technology
University of Chinese Academy of Sciences
Beijing 101408, China
E-mail: huihuang@ucas.ac.cn
Prof. W. Li
CAS Key Laboratory of Organic Solids
Institute of Chemistry Chinese Academy of Sciences
Beijing 100190, China

**ADVANCED
SCIENCE NEWS**
www.advancedsciencenews.com

**ADVANCED
FUNCTIONAL
MATERIALS**
www.afm-journal.de

incorporation of n-doping agent $NaBH_4$ to increase or decrease the work function of TMD nanosheets. Obviously, this post-treatment is costly for commercial applications.

Here, PEDOT:PSS is selected as an effective exfoliating agent to prepare single- and few-layer graphene and TMDs. This method is safe, scalable, and efficient, which can be carried out at ambient conditions. Furthermore, the one-pot-prepared PEDOT:PSS/WS_2 ink can be employed as an efficient HEL for OSCs, which can enhance charge carrier mobility due to the "island" morphology and the increased conductivity. As a result, the PEDOT:PSS/WS_2-based OSCs exhibit PCE as high as 7.24%, which is superior to those based on pristine PEDOT:PSS. Moreover, the stability of OSCs based on PEDOT:PSS/WS_2 is greatly improved due to the incorporation of WS_2 nanosheets.

Figure 1. Optical images of exfoliated A) P-MoS_2 suspension in aqueous solution after sonication for different times. The phenomenon of Tyndall effect for B) P-MoS_2 dispersion after dilution. UV–vis absorption spectra of the exfoliated C) P-MoS_2 nanosheets in water after sonication for different times. D) PL spectra of PEDOT:PSS after dilution (at 250 nm excitation), P-MoS_2, P-WS_2, and P-graphene aqueous solution. For clarity, the spectra for P-MoS_2 and P-WS_2 are shifted vertically.

2. Results and Discussion

After sonicating in a sonic bath, single- and few-layer nanosheets were obtained in aqueous solution, as displayed in **Figure 1**A,B (Figure S1, Supporting Information), after removing unexfoliated flakes and free PEDOT:PSS by repeatedly washing with deionized water. The color of suspension became darker with the increasing sonication time, indicating that the amount of exfoliated nanosheets increases with the sonication time. Furthermore, the colloidal dispersion displays an obvious Tyndall effect (Figure 1B), suggesting the successful exfoliation of these layered materials, which is stable for over 1 month. UV–vis absorption spectra of P-MoS_2, P-WS_2, and P-graphene aqueous solution were employed to monitor the sonication of the graphite/TMD powder (Figure 1C; Figure S2, Supporting Information). For P-MoS_2 nanosheets as shown in Figure 1C, there are four characteristic peaks locating at 395, 455, 615, and 676 nm. The peaks at 395 and 455 nm arise from the direct transition from the deep valence band to the conduction band, while the peaks at 615 and 676 nm are attributed to the K point of the Brillouin zone.[34,35] The intensity of all these characteristic peaks became stronger with the increasing time. By using Lambert–Beer law and the extinction coefficient at 600 nm α_{600} = 2104 mL (mg m)$^{-1}$,[20] the concentration is estimated to be 0.16 mg mL^{-1}, which is comparable to the reported yield by sonication by other surfactants such as sodium cholate[16] and poloxamers.[20] Since partial P-MoS_2 was lost during the repeated washing, the actual concentration may be even higher. Note that the absorption peaks of PEDOT:PSS at 224 and 270 nm (Figure S3, Supporting Information) were observed in exfoliated nanosheets, indicating that the nanosheets are covered and noncovalently functionalized with a layer of PEDOT:PSS. To further reveal the exfoliation mechanism, photoluminescence spectra were obtained, as illustrated in Figure 1D. PEDOT:PSS shows two emission peaks at 370 and 580 nm under irradiation at 250 nm, while these emissions were totally quenched in exfo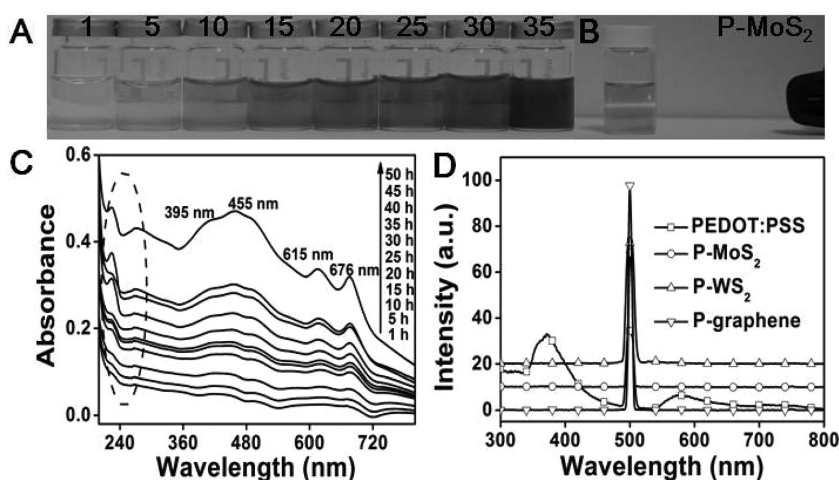liated nanosheets in aqueous solution. This is attributed to the fact that the π–π interaction between PEDOT:PSS and nanosheets leads to adsorption of PEDOT:PSS onto surface of the exfoliated nanosheets. The effective electron or energy transfer between PEDOT:PSS and exfoliated nanosheets[36,37] accounts for the observed PL quenching.

The morphological characteristics of exfoliated nanosheets were investigated by transmission electron microscope (TEM) and atomic force microscopy (AFM) as shown in **Figure 2**. TEM images demonstrated that the exfoliated nanosheets have an average size of ≈100 nm. The selected area electron diffraction (SAED) images of P-MoS_2 and P-WS_2 (Figure 2C,D) exhibited a single-crystalline hexagonal spot pattern, indicating the retained crystalline nature of the exfoliated nanosheets. The d-spacings of exfoliated nanosheets are 0.27 and 0.27 nm, attributed to the (100) planes of MoS_2 and WS_2, respectively.[17] We tried our best to observe the high-resolution TEM (HRTEM) image for P-graphene; however, we failed. This may be because the graphene composed of light carbon atoms is easy to be damaged by electron beam. The thickness of P-MoS_2 and P-WS_2 was measured to be 1 and 0.65 nm, respectively, suggesting that TMD nanosheets with single-layer structure were obtained, since the TMD monolayer is about 1 nm.[9,22] However, the P-graphene has a thickness of about 3–4 layers. Previously, Guan et al.[19] found that different functional groups on bovine serum albumin have different binding capability on graphite and TMD materials. Thus, the different thickness of P-graphene and P-MoS_2/WS_2 may also be reasonably attributed to the different binding capability of PEDOT:PSS on graphite and TMDs. Note that the adsorbed PEDOT:PSS is easily identified from the underlying nanosheets as light spot with average thickness of ≈15 nm, which are similar to reported results.[19,21] The amount of PEDOT:PSS absorbed on nanosheets is measured by thermogravimetric analysis (TGA) to be about 20% (Figure S4, Supporting Information).
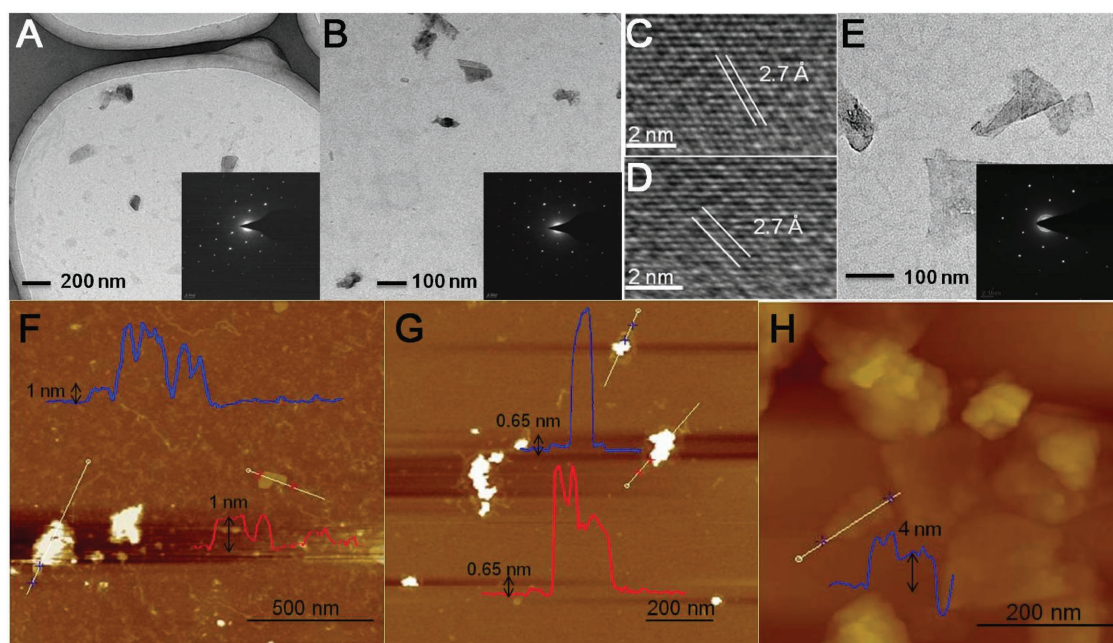
ADVANCED
SCIENCE NEWS
www.advancedsciencenews.com

ADVANCED
FUNCTIONAL
MATERIALS
www.afm-journal.de

Figure 2. TEM image of A) P-MoS$_2$, B) P-WS$_2$, and E) P-graphene nanosheets. The inset is the corresponding SAED pattern. HRTEM images of C) P-MoS$_2$ and D) P-WS$_2$ nanosheets. AFM images of F) P-MoS$_2$, G) P-WS$_2$, and H) P-graphene nanosheets.

Raman spectra and X-ray diffraction (XRD) spectra as shown in **Figure 3**A–F also confirmed the well-exfoliated nature of nanosheets. Raman spectra of graphene/TMD appear to contain two characteristic peaks, namely the out-of-plane (A$_{1g}$) mode and the in-plane (E$^1_{2g}$) mode. The location and wavenumber difference of these two peaks are closely related to the

thickness of the nanosheets.[17] For P-MoS$_2$ nanosheets, these two characteristic peaks show apparent blue shift compared to those of its bulk crystal. Meanwhile, the wavenumber difference from 26 cm^{-1} for bulk MoS$_2$ decreases to 25 cm^{-1} for P-MoS$_2$ nanosheets. Note that the gap distance of MoS$_2$ produced by micromechanical exfoliation with mono or bilayer
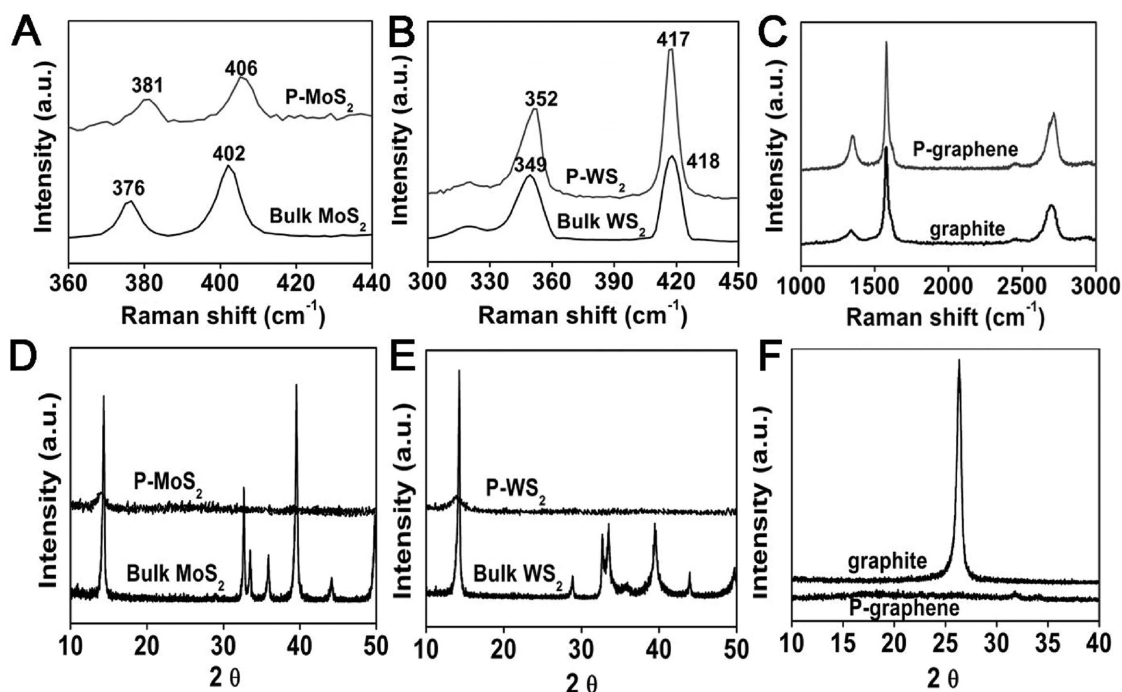

Figure 3. Raman spectra of A) P-MoS$_2$, B) P-WS$_2$, and C) P-graphene nanosheets and their corresponding bulk crystals. XRD spectra of D) P-MoS$_2$, E) P-WS$_2$, and F) P-graphene nanosheets and their corresponding bulk crystals.

ADVANCED
SCIENCE NEWS
www.advancedsciencenews.com
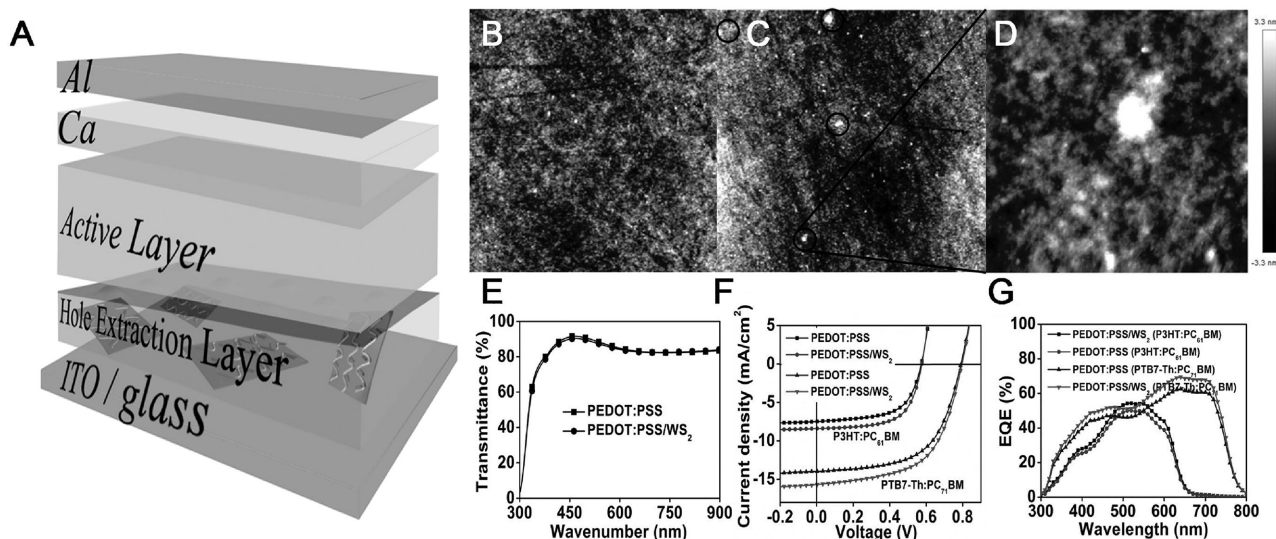
ADVANCED
FUNCTIONAL
MATERIALS
www.afm-journal.de

Figure 4. A) Device structure of OSC. AFM topographic images of B) PEDOT:PSS and C) PEDOT:PSS/WS$_2$ film on ITO/glass substrates. The circles represent P-WS$_2$ underlying in PEDOT:PSS. D) Enlarged image from panel (C). E) The transmittance spectra of PEDOT:PSS and PEDOT:PSS/WS$_2$. F) J–V curves based on the active layer of P3HT:PC$_{61}$BM and PTB7-Th:PC$_{71}$BM, respectively. G) EQE curves of P3HT:PC$_{61}$BM and PTB7-Th:PC$_{71}$BM based on different HELs. The size in panels (B) and (C) is 8×8 μm^2 and the size in panel (D) is 1×1 μm^2.

structure shows <20 and <22 cm^{-1}.[38] However, besides the layer number, surface adsorption can also have an effect on this gap distance. Large gap distance between A$_{1g}$ and E$^1_{2g}$ with the range of 24–26 cm^{-1} was also observed in the experiments based on exfoliation with surfactants.[17,19,39] In regards to the blue shift, the interaction between PEDOT:PSS and 2D nanosheets combined with the restacking of nanosheets complicates the Raman analysis. Note that a similar blue shift was observed by other researchers, altthough the reasons are unknown.[17,39] We consider that the interaction between PEDOT:PSS and 2D nanosheets may play an important role in the blue shift, which needs to be further investigated. As to P-WS$_2$, A$_{1g}$, and E$^1_{2g}$, peaks shifted to a decreased and increased wavenumber, respectively, which is also in line with reported results.[17,40] For P-graphene, there are typically three characteristic peaks containing a defect-related D band at ≈1350 cm^{-1}, G band at 1580 cm^{-1} attributed to vibration of the sp^2-hybridized carbon atoms, and the second order of the D band (2D band) at ≈2700 cm^{-1}.[41] The intensity ratio of D band to G band (I_D/I_G) is often used to indicate the defects level in the carbon materials.[42] This value increased from 0.13 for bulk graphite to 0.28 for P-graphene, suggesting more sonication-induced basal plane defects and/or edge defects.[43] The successful exfoliation of single- and few-layer structure can be confirmed further by XRD. For P-MoS$_2$, XRD spectra showed none of the characteristic peaks of bulk MoS$_2$ besides the (002) peak, illustrating formation of few-layer nanosheets.[17,44] For P-WS$_2$ and P-graphene, similar phenomena are observed that the peak assigned to (002) weakens or even disappears.

To demonstrate that these graphene/TMD nanosheets exfoliated by PEDOT:PSS-assisted method can be used as nanofiller to replace PEDOT:PSS, PEDOT:PSS/WS$_2$ hybrid ink was prepared by simple centrifugation and directly used as a model HEL to fabricate OSCs. AFM of both PEDOT:PSS and PEDOT:PSS/WS$_2$ film was carried out. After the deposition of PEDOT:PSS, the

root-mean-square (RMS) roughness was 0.78 nm. The RMS of PEDOT:PSS/WS$_2$ film increases to 0.97 nm, indicating a slightly rougher surface compared with that of PEDOT:PSS. It is worth noting that small islands with a feature of ≈100 nm can be observed in the enlarged **Figure** 4C. The 3D image and SEM (Figure S5, Supporting Information) can further consolidate existence of the islands. Given that these sizes are in consistent with the size range observed in Figure 2, these islands were assigned to P-WS$_2$ nanosheets. The "island" morphology may extend the contact area between the active layer and PEDOT:PSS/WS$_2$, allowing for efficient hole collection.[45,46] Figure 4D shows almost similar transmittance between PEDOT:PSS/WS$_2$ and PEDOT:PSS, allowing for the adequate absorption of sunlight.

Poly(3-hexylthiophene):(6,6)-phenyl-C$_{61}$ butyric acid methyl ester (P3HT:PC$_{61}$BM)-based solar cells were first investigated to understand the effects of incorporation of TMD nanosheets on photovoltaic performances. The OSC structure is ITO/HEL(30 nm)/P3HT:PC$_{61}$BM(100 nm)/Ca(20 nm)/Al(100 nm). The typical J–V curves measured from devices under AM 1.5 G illumination are shown in Figure 4E and the photovoltaic parameters are summarized in **Table 1**. It can be observed that the controlled devices with PEDOT:PSS show an open voltage (V_{oc}) of 0.57 V, short circuit current (J_{sc}) of 7.49 mA cm^{-2}, fill factor (FF) of 61.40%, and a PCE of 2.61%. Significantly, the devices based on PEDOT:PSS/WS$_2$ afford V_{oc} of 0.57 V, J_{sc} of 8.39 mA cm^{-2}, FF of 64.6%, and a PCE of 3.07%, ≈20% higher than that of PEDOT:PSS-based devices. To investigate the versatility of PEDOT:PSS/WS$_2$ as HELs for OPVs, poly[[2,6′-4,8-di(5-ethylhexylthienyl)benzo[1,2-b;3,3-b] dithiophene] [3-fluoro-2[(2-ethylhexyl)carbonyl]thieno[3,4-b]thiophenediyl]]:(6,6)-phenyl-C$_{71}$ butylric acid methyl ester (PTB7-Th:PC$_{71}$BM)-based OSCs were also studied. The devices based on PEDOT:PSS/WS$_2$ exhibit a remarkable efficiency of 7.24%, with V_{oc} of 0.79 V, J_{sc} of 15.67 mA cm^{-2}, FF of 58.6%. Again, this efficiency is over 10% higher than the PEDOT:PSS-based devices, which exhibit a PCE

**ADVANCED
SCIENCE NEWS**
www.advancedsciencenews.com

**ADVANCED
FUNCTIONAL
MATERIALS**
www.afm-journal.de

Table 1. Photovoltaic parameters of OSCs.

Active layer	HEL	V_{OC} [V]	J_{SC} [mA cm^{-2}]	FF [%]	PCE [%]	R_s [Ω cm^2]
P3HT:PC$_{61}$BM	PEDOT:PSS	0.57 ± 0.01	7.49 ± 0.13	61.40 ± 0.11	2.61 ± 0.11	3.46
	PEDOT:PSS/WS$_2$	0.57 ± 0.01	8.39 ± 0.15	64.62 ± 0.13	3.07 ± 0.04	3.10
PTB7-Th: PC$_{71}$BM	PEDOT:PSS	0.79 ± 0.01	14.25 ± 0.22	58.27 ± 0.21	6.56 ± 0.09	2.76
	PEDOT:PSS/WS$_2$	0.79 ± 0.01	15.67 ± 0.19	58.60 ± 0.14	7.24 ± 0.13	2.63

of 6.53%, V_{oc} of 0.79 V, J_{sc} of 14.25 mA cm^{-2}, FF of 58.27%. These results showed the superiority of PEDOT:PSS/WS$_2$ over PEDOT:PSS as HEL. Obviously, the enhanced PCE is mainly attributed to the increased J_{sc} and FF in both OSC systems. The increased J_{sc} is also supported by the higher external quantum efficiency (EQE) of PEDOT:PSS/WS$_2$-based devices than that of PEDOT:PSS-based ones in both P3HT:PC$_{61}$BM and PTB7-Th:PC$_{71}$BM active layer (Figure 4F).

To probe the mechanism of enhanced performance of PEDOT:PSS/WS$_2$-based OSCs, four-point-probe measurements were carried out to evaluate the conductivity of PEDOT:PSS and PEDOT:PSS/WS$_2$ films. The conductivity of PEDOT:PSS/WS$_2$ is 14.3 × 10^{-4} S cm^{-1}, which is 2.5 times that of pristine PEDOT/PSS film (5.7 × 10^{-4} S cm^{-1}). The enhanced conductivity of the PEDOT:PSS/WS$_2$ in relation to the hole transport is confirmed by the space charge-limited current (SCLC) regime of device in **Figure 5**A. The effective hole mobility (μ_h) of the hole-only device with PEDOT:PSS, using the Mott–Gurney Law, is calculated to be 6.54 × 10^{-6} cm^2 V^{-1} S^{-1}, while μ_h for PEDOT:PSS/WS$_2$ increased to 1.73 × 10^{-5} cm^2 V^{-1} S^{-1}. This observation is consistent with the enhancement of the FF for PEDOT:PSS/WS$_2$-based devices. Furthermore, the dark J–V characteristics of OSCs based on PEDOT:PSS and PEDOT:PSS/WS$_2$ are shown in Figure 5B. It

was found that the dark current densities of PEDOT:PSS/WS$_2$-based OSCs are approximately one order lower than those of PEDOT:PSS-based devices. The low dark current density indicates the suppression of bimolecular recombination, resulting in high photocurrent.[47] Based on the experimental observations, a possible PEDOT:PSS-assisted exfoliation mechanism was proposed. After incorporation of graphite/TMD crystals into PEDOT:PSS solution, PEDOT:PSS can adsorb onto the surface of the graphite/TMD crystals and act as surfactant to help the dispersion of TMD crystal in water. Upon the shear force imposed by sonication, the PEDOT:PSS-adsorbed layer of graphene/TMD nanosheets may slide from its below layers and PEDOT:PSS again adsorb on the surface of freshly exposed layer. The process proceeds repeatedly to produce single- and few-layer graphene/TMD nanosheets stabilized by PEDOT:PSS. Meanwhile, the conformation of PEDOT:PSS changes from coil to linear due to the π–π interaction between PEDOT and graphene/TMD nanosheets.[48] The conformational structure of PEDOT changes from benzoid to quinoid, which is validated by the red shift from 1441 to 1434 cm^{-1} in Figure 5C. The benzoid–quinoid transition is favorable for the conductivity improvement,[49] which is consistent with the conductivity measurement result. Moreover, the stability of the PEDOT:PSS and PEDOT:PSS/WS$_2$-based OSCs was investigated in the N$_2$ glove box at 25 °C (Figure 5D). After 36 d, PEDOT:PSS/WS$_2$-based OSCs kept 77.3% of the initial PCE while PEDOT:PSS-based OSCs decreased to 66.1%. The acidity of PEDOT:PSS leads to faster device degradation while the layered WS$_2$ can alleviate the corrosion of PEDOT:PSS toward indium tin oxide (ITO) and active layer, resulting in enhanced stability.

3. Conclusion

In conclusion, we have successfully prepared single- and few-layer graphene/TMD nanosheets through exfoliating the bulk 2D materials with PEDOT:PSS solution. The one-pot prepared hybrid ink can be used as an effective HEL to enhance the PCE and the stability of OSCs. The results showed that the improved conductivity of TMD nanosheets may enhance the charge transport between the interfacial layers. This work reports a novel method to prepare single- and few-layer graphene/TMD and paves the way for the applications of TMD/conjugated polymers nanocomposite.
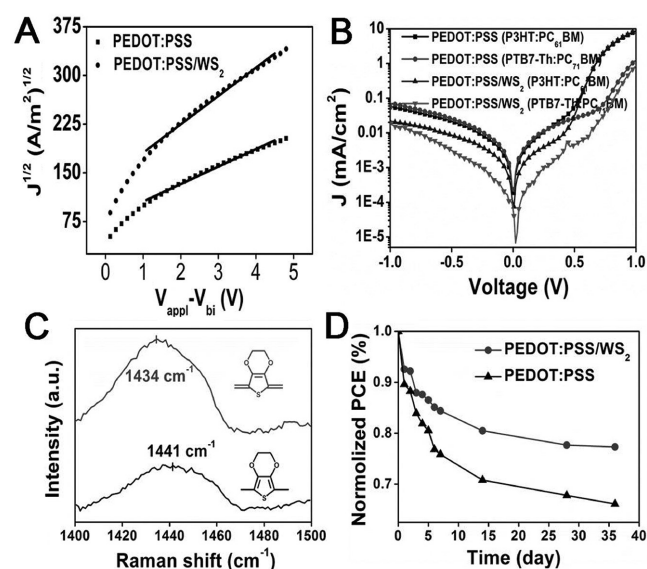

Figure 5. A) The representative J–V curves in dark for hole-only device with different HELs in between ITO and Au electrodes. The lines show fits to the SCLC regions. B) Dark J–V characteristics of devices with different HELs based on P3HT:PC$_{61}$BM and PTB7-Th:PC$_{71}$BM active layer. C) Raman spectra of PEDOT:PSS and PEDOT:PSS/WS$_2$. D) Stability of device with different HELs based on P3HT:PC$_{61}$BM active layer.

4. Experimental Section

Materials: All 2D materials were purchased in powder form. The raw materials were as follows: MoS$_2$ (Aldrich, <2 μm, 99%), WS$_2$ (Aladdin, ≈2 μm, 99.9%), and graphite (Ruisheng graphite Co. Ltd., ≈1 μm).

**ADVANCED
SCIENCE NEWS**

www.advancedsciencenews.com

**ADVANCED
FUNCTIONAL
MATERIALS**

www.afm-journal.de

Exfoliation: 100 mg of MoS_2 was added into 10 mL of PEDOT:PSS aqueous solution (Baytron P VP AI 4083) and the mixture was sonicated (KQ3200DE, Kunshan Ultrasonic Instruments Co. Ltd.) for 48 h in ice-water bath. The resulting suspension was settled overnight without disturbance. Afterward, the top dispersion was centrifuged at 5000 rpm for 60 min to collect precipitant, which was redispersed into water by light sonication. Furthermore, the mixture was centrifuged at 1500 rpm for 60 min to discard the unexfoliated flakes. Afterward, the supernatant was decanted and centrifuged again at 12 000 rpm for 15 min and the sediment was redispersed in water. The process was repeated for several times until the supernatant became colorless. The final sediment MoS_2 nanosheets were obtained and remarked as P-MoS_2. Similarly, WS_2 and graphite were used to replace MoS_2 and underwent the identical procedure. To obtain HEL ink for OSCs, the WS_2 dispersion after sonication underwent centrifugation at 10 000 rpm for 30 min and the supernatant denoted as PEDOT:PSS/WS_2 was directly integrated into OSCs.

Fabrication and Characterization of OSCs: The indium tin oxide-coated glass substrates were cleaned sequentially with detergent water, deionized water, acetone, hexane, and isopropanol with sonication assistance, followed by exposing to UV–ozone treatment for 30 min. The PEDOT:PSS or PEDOT:PSS/WS_2 solution was spun-coated on ITO substrate at 4000 rpm for 40 s, followed by heating at 140 °C for 20 min. The active layer PTB7-Th:$PC_{71}BM$ with weight ratio 1:1.5 (10 mg mL^{-1} of PTB7-Th in chlorobenzene with 3 vol% 1,8-diiodineoctane) or P3HT:$PC_{61}BM$ with weight ratio 1:1 (10 mg mL^{-1} of P3HT in chlorobenzene) was spun-coated on top of the HEL layer. Finally, the Ca (20 nm) and cathode Al (100 nm) were thermally deposited onto the active layer under the pressure of 1×10^{-6} Torr. All J–V characterizations were performed under AM 1.5 G using a Newport solar simulator. The effective area for the cells is 4 mm^2.

Characterization: Atomic force microscopy (NTEGRA Solaris) was used to characterize the morphology of the nanosheets. The suspension was deposited on fresh mica by spin coating and dried under ambient condition. AFM images were obtained in a tapping mode. Transmission electron microscope (FEI Tecnai G2 F20 S-TWIN) was observed at an accelerating voltage of 200 kV. The surface morphology was examined by a field-emission scanning electron microscopy (SU8020, Hitachi, Japan). Raman spectroscopy was performed using in Via-Reflex with 532 nm excitation laser in air under ambient conditions. UV–visible absorption and photoluminescence spectra were carried out with a Cary 60 spectrometer and a Cary Eclipse spectrometer, respectively. X-ray diffraction were characterized by an X-ray diffractometer (XD-3, PERSEE). Thermogravimetric analysis was carried out on a TGA Q600 under nitrogen atmosphere with a heating rate of 10 °C min^{-1}.

Supporting Information

Supporting Information is available from the Wiley Online Library or from the author.

Acknowledgements

Conflict of Interest

The authors declare no conflict of interest.

Keywords

[1] K. Novoselov, A. Geim, S. Morozov, D. Jiang, Y. Zhang, S. Dubonos, I. Grigorieva, A. Firsov, *Science* **2004**, *306*, 666.

[2] D. McManus, S. Vranic, F. Withers, V. Romaguera, M. Macucci, H. Yang, R. Sorrentino, K. Parvez, S. Son, G. Iannaccone, K. Kostarelos, G. Fiori, C. Casiraghi, *Nat. Nanotechnol.* **2017**, *12*, 343.

[3] G. Frey, S. Elani, M. Homyonfer, Y. Feldman, R. Tenne, *Phys. Rev. B* **1998**, *57*, 6666.

[4] J. Chang, L. Register, S. Banerjee, *Appl. Phys. Lett.* **2013**, *103*, 223509.

[5] X. Li, W. Zhang, Y. Wu, C. Min, J. Fang, *ACS Appl. Mater. Interfaces* **2013**, *5*, 8823.

[6] K. Kwon, C. Kim, Q. Le, S. Gim, J. Jeon, J. Ham, J. Lee, H. Jang, S. Kim, *ACS Nano* **2015**, *9*, 4146.

[7] K. Novoselov, D. Jiang, F. Schedin, T. Booth, V. Khotkevich, S. Morozov, A. Geim, *Proc. Natl. Acad. Sci. USA* **2005**, *102*, 10451.

[8] J. Zheng, H. Zhang, S. Dong, Y. Liu, C. Nai, H. Shin, H. Jeong, B. Liu, K. Loh, *Nat. Commun.* **2014**, *5*, 2995.

[9] H. Feng, Z. Hu, X. Liu, *Chem. Commun.* **2015**, *51*, 10961.

[10] P. Joensen, R. Frindt, S. Morrison, *Mater. Res. Bull.* **1986**, *21*, 457.

[11] Z. Zeng, Z. Yin, X. Huang, H. Li, Q. He, G. Lu, F. Boey, H. Zhang, *Angew. Chem., Int. Ed.* **2011**, *50*, 11093.

[12] J. Coleman, M. Lotya, A. O'Neill, S. Bergin, P. King, U. Khan, K. Young, A. Gaucher, S. De, R. Smith, I. Shvets, S. Arora, G. Stanton, H. Kim, K. Lee, G. Kim, G. Duesberg, T. Hallam, J. Boland, J. Wang, J. Donegan, J. Grunlan, G. Moriarty, A. Shmeliov, R. Nicholls, J. Perkins, E. Grieveson, K. Theuwissen, D. McComb, P. Nellist, V. Nicolosi, *Science* **2011**, *331*, 568.

[13] C. Backes, B. Szydłowska, A. Harvey, S. Yuan, V. Mayoral, B. Davies, P. Zhao, D. Hanlon, E. Santos, M. Katsnelson, W. Blau, C. Gadermaier, J. Coleman, *ACS Nano* **2016**, *10*, 1589.

[14] Y. Fang, Y. Lv, F. Gong, A. Elzatahry, G. Zheng, D. Zhao, *Adv. Mater.* **2016**, *28*, 9385.

[15] X. Rocquefelte, F. Boucher, P. Gressier, G. Ouvrard, P. Blaha, K. Schwarz, *Phys. Rev. B* **2000**, *62*, 2397.

[16] R. Smith, P. King, M. Lotya, C. Wirtz, U. Khan, S. De, A. O'Neill, G. Duesberg, J. Grunlan, G. Moriarty, J. Chen, J. Wang, A. Minett, V. Nicolosi, J. Coleman, *Adv. Mater.* **2011**, *23*, 3944.

[17] L. Niu, K. Li, H. Zhen, Y. Chui, W. Zhang, F. Yan, Z. Zheng, *Small* **2014**, *10*, 4651.

[18] Y. Chen, C. Wu, T. Kuo, Y. Chang, M. Jen, I. Chen, *Sci. Rep.* **2016**, *6*, 26660.

[19] G. Guan, S. Zhang, S. Liu, Y. Cai, M. Low, C. Teng, I. Phang, Y. Cheng, K. Duei, B. Srinivasan, Y. Zheng, Y. Zhang, M. Han, *J. Am. Chem. Soc.* **2015**, *137*, 6152.

[20] N. Mansukhani, L. Guiney, P. Kim, Y. Zhao, D. Alducin, A. Ponce, E. Larios, M. Yacaman, M. Hersam, *Small* **2016**, *12*, 294.

[21] Z. Lei, Y. Zhou, P. Wu, *Small* **2016**, *12*, 3112.

[22] V. Mayoral, C. Backes, D. Hanlon, U. Khan, Z. Gholamvand, M. O'Brien, G. Duesberg, C. Gadermaier, J. Coleman, *Adv. Funct. Mater.* **2016**, *26*, 1028.

[23] J. Li, M. Naiini, S. Vaziri, M. Lemme, M. Östling, *Adv. Funct. Mater.* **2014**, *24*, 6524.

[24] M. Jørgensen, K. Norrman, F. Krebs, *Sol. Energy Mater. Sol. Cells* **2008**, *92*, 686.

**ADVANCED
SCIENCE NEWS**

www.advancedsciencenews.com

**ADVANCED
FUNCTIONAL
MATERIALS**

www.afm-journal.de

[25] J. Liu, G. Kim, Y. Xue, J. Kim, J. Baek, M. Durstock, L. Dai, *Adv. Mater.* **2014**, *26*, 786.

[26] X. Gu, W. Cui, H. Li, Z. Wu, Z. Zeng, S. Lee, H. Zhang, B. Sun, *Adv. Energy Mater.* **2013**, *3*, 1262.

[27] Q. Le, T. Nguyen, H. Jang, S. Kim, *Phys. Chem. Chem. Phys.* **2014**, *16*, 13123.

[28] P. Qin, G. Fang, W. Ke, F. Cheng, Q. Zheng, J. Wan, H. Lei, X. Zhao, *J. Mater. Chem. A* **2014**, *2*, 2742.

[29] X. Yang, W. Fu, W. Liu, J. Hong, Y. Cai, C. Jin, M. Xu, H. Wang, D. Yang, H. Chen, *J. Mater. Chem. A* **2014**, *2*, 7727.

[30] J. Yun, Y. Noh, C. Lee, S. Na, S. Lee, S. Jo, H. Joh, D. Kim, *Small* **2014**, *10*, 2319.

[31] M. Ibrahem, T. Lan, J. Huang, Y. Chen, K. Wei, L. Li, C. Chu, *RSC Adv.* **2013**, *3*, 13193.

[32] J. Yun, Y. Noh, J. Yeo, Y. Go, S. Na, H. Jeong, J. Kim, S. Lee, S. Kim, H. Koo, T. Kim, D. Kim, *J. Mater. Chem. C* **2013**, *1*, 3777.

[33] W. Xing, Y. Chen, X. Wang, L. Lv, X. Ouyang, Z. Ge, H. Huang, *ACS Appl. Mater. Interfaces* **2016**, *8*, 26916.

[34] W. Dai, W. Dong, B. Fugetsu, Y. Cao, H. Lu, X. Ma, X. Zhang, *Small* **2015**, *11*, 4158.

[35] T. Wang, L. Liu, Z. Zhu, P. Papakonstantinou, J. Hu, H. Liu, M. Li, *Energy Environ. Sci.* **2013**, *6*, 625.

[36] Y. Xu, H. Bai, G. Lu, C. Li, G. Shi, *J. Am. Chem. Soc.* **2008**, *130*, 5856.

[37] C. Backes, C. Schmidt, F. Hauke, C. Böttcher, A. Hirsch, *J. Am. Chem. Soc.* **2009**, *131*, 2172.

[38] C. Lee, H. Yan, L. Brus, T. Heinz, J. Hone, S. Ryu, *ACS Nano* **2010**, *4*, 2695.

[39] X. Yu, M. Prévot, K. Sivula, *Chem. Mater.* **2014**, *26*, 5892.

[40] Y. Zhang, Y. Zhang, Q. Ji, J. Ju, H. Yuan, J. Shi, T. Gao, D. Ma, M. Liu, Y. Chen, X. Song, H. Hwang, Y. Cui, Z. Liu, *ACS Nano* **2013**, *7*, 8963.

[41] M. Pimenta, G. Dresselhaus, M. Dresselhaus, L. Cancado, A. Jorio, R. Saito, *Phys. Chem. Chem. Phys.* **2007**, *9*, 1276.

[42] U. Khan, A. O'Neill, M. Lotya, S. De, J. Coleman, *Small* **2010**, *6*, 864.

[43] Y. Liu, X. Xie, X. Ye, *Carbon* **2011**, *49*, 3529.

[44] F. Jiang, J. Xiong, W. Zhou, C. Liu, L. Wang, F. Zhao, H. Liu, J. Xu, *J. Mater. Chem. A* **2016**, *4*, 5265.

[45] V. Shrotriya, G. Li, Y. Yao, C. Chu, Y. Yang, *Appl. Phys. Lett.* **2006**, *88*, 073508.

[46] Y. Sun, C. Takacs, S. Cowan, J. Seo, X. Gong, A. Roy, A. Heeger, *Adv. Mater.* **2011**, *23*, 2226.

[47] T. Yang, M. Wang, C. Duan, X. Hu, L. Huang, J. Peng, F. Huang, X. Gong, *Energy Environ. Sci.* **2012**, *5*, 8208.

[48] G. Kim, D. Hwang, S. Woo, *Phys. Chem. Chem. Phys.* **2012**, *14*, 3530.

[49] J. Ouyang, Q. Xu, C. Chu, Y. Yang, G. Li, J. Shinar, *Polymer* **2004**, *45*, 8443.

1701622 (7 of 7)